Excitations in the spin-1 trimer chain compound $CaNi_3P_4O_{14}$: From gapped dispersive spin waves to gapless magnetic excitations

A. K. Bera,[1] S. M. Yusuf,[1,2,*] and D. T. Adroja[3,4]

[1]*Solid State Physics Division, Bhabha Atomic Research Centre, Mumbai 400085, India*

[2]*Homi Bhabha National Institute, Anushaktinagar, Mumbai 400094, India*

[3]*ISIS Facility, STFC Rutherford Appleton Laboratory, Harwell Oxford, Didcot OX11 0QX, United Kingdom*

[4]*Highly Correlated Matter Research Group, Department of Physics, University of Johannesburg, Auckland Park 2006, South Africa*

(Received 28 March 2018; revised manuscript received 18 May 2018; published 13 June 2018)

Magnetic excitations and the spin Hamiltonian of the spin-1 trimer chain compound $CaNi_3P_4O_{14}$ have been investigated by inelastic neutron scattering. The trimer spin chains in $CaNi_3P_4O_{14}$ result from the crystal structure that provides a special periodicity of the exchange interactions (J_1-J_1-J_2) comprising intratrimer (J_1) and intertrimer (J_2) exchange interactions along the crystallographic b axis. Experimental data reveal gapped dispersive spin-wave excitations in the 3D long-range ordered magnetic state ($T_C = 16$ K), and gapless magnetic excitations above the T_C due to the low-dimensional spin-spin correlations within chains. Simulated magnetic excitations, by using the linear spin-wave theory, for a model of coupled trimer spin chains provide a good description of the observed experimental data. The analysis reveals both ferromagnetic J_1 and J_2 interactions within the chains, and an antiferromagnetic interchain interaction J_3 between chains. The strengths of the J_1 and J_2 are found to be closer ($J_2/J_1 \sim 0.81$), and J_3 is determined to be weaker ($|J_3/J_1| \sim 0.69$), which is consistent with the spin-chain-type crystal structure. Presence of a weak single-ion anisotropy ($D/J = 0.19$) is also revealed. The strengths and signs of exchange interactions explain why the 1/3 magnetization is absent in the studied spin-1 compound $CaNi_3P_4O_{14}$ in contrast to its $S = 5/2$ counterpart Mn-based isostructural compound. The signs of the exchange interactions are in agreement with that obtained from the reported density-functional theory calculations, whereas their strengths are found to be significantly different. The relatively strong value of the J_3 in $CaNi_3P_4O_{14}$ gives a conventional 3D-type magnetic ordering behavior below the T_C with full ordered moment at 1.5 K, however, retains its 1D character above the T_C. The present experimental study also reveals a sharp change of single-ion anisotropy across the T_C, indicating that the stability of the 3D magnetic ordering in $CaNi_3P_4O_{14}$ is ascribed to the local magnetic anisotropy in addition to interchain interactions. The present study divulges the importance of full knowledge of the exchange interactions in trimer spin-chain compounds to understand their exotic magnetic properties, such as 1/3 magnetization plateau. The importance of the observed gapless magnetic excitations of the strongly correlated spin chains above the T_C is also discussed.

DOI: 10.1103/PhysRevB.97.224413

I. INTRODUCTION

Low-dimensional magnetic materials, in particular one-dimensional (1D) spin chains, are currently of great interest in condensed-matter physics as model experimental systems to study the physics of many-body quantum physics [1]. In general, the magnetic ordering in 1D spin systems is suppressed even at $T = 0$ K by strong quantum fluctuations. Further, the ground-state and low-lying excitations of half-integer spin chains are completely different from those for integer spin chains [2,3]. Coupled spin chains are of further interest as the interchain couplings lead to unusual magnetic properties, and can even stabilize magnetic ordering (beyond the critical value of the interchain coupling) with diverse characteristics [4,5]. Further, spin-chain systems consisting of multiple intrachain interactions, such as alternating [6], dimer [7], trimer [8], and tetramer [9] spin chains, have recently attracted much attention due to their various unconventional magnetic properties that originate from the periodicity of exchange interactions within the chains [10].

Among the aforementioned systems, the trimer spin chains are of special interest to us. Trimer units are formed by three consecutive atomic spins which are coupled by strong intratrimer exchange interactions J_1's. A trimer spin chain is formed by interconnecting trimers in the one dimension with intertrimer exchange interaction J_2, which leads to periodic exchange interactions J_1-J_1-J_2. Among the diverse properties of trimer spin chains, the occurrence of the magnetization plateaus, which can be viewed as an essentially macroscopic quantum phenomenon, has gained much attention recently. Analogous to the quantum Hall effect, at the magnetization plateau state magnetization is quantized to fractional values of the saturated magnetization value, proving a striking example of the macroscopic quantum phenomenon. In the trimer spin-chain systems, the presence of magnetization plateaus is theoretically predicted for a wide range of interactions strengths of J_1 and J_2 as well as spin values where the number of the plateaus ($2S + 1$) strongly depends on the spin value S [11]. The appearance of the plateaus is theoretically predicted

*smyusuf@barc.gov.in

for both ferromagnetic (FM) and antiferromagnetic (AFM) intratrimer interactions J_1 with FM-FM-AFM and AFM-AFM-FM/AFM configurations [11]. It is also predicted that apart from the signs of the J_1 and J_2, the nature of the magnetic ground state and the appearance of the magnetization plateau states are also dependent on the relative strength (J_2/J_1) of the intrachain interactions, interchain interactions (J_3), spin values, as well as anisotropy in trimer spin chains. The ground state for an AFM trimer chain (AFM J_1) with an integer spin is theoretically predicted to be trimerized and a gap is predicted between the ground state and the first excited state for an extended range of exchange interactions strengths [12]. On the other hand, the ground state for the half-integer counterpart is degenerate [13]. It was theoretically reported that, for AFM-AFM-FM trimer chain the magnetization plateaus appear only below a critical value of $|J_2/J_1|$, whereas for FM-FM-AFM trimer spin chain, plateaus appear above a critical value of $|J_2/J_1|$. In both the cases, the essential condition for the plateau state to be observed is the dominating AFM interactions. Therefore, knowledge of the sign and strength of the exchange interactions J_1 and J_2 is essential for a trimer spin-chain compound to understand microscopically the presence or absence of magnetization plateaus as well as their nature. It is also essential to know the ratios of the exchange interactions (J_1, J_2 and J_3) which determine how good or bad a system to be considered is as a trimer system as well as to correlate with their physical properties.

However, experimental studies on model spin-trimer chain compounds are limited. Among the experimentally reported compounds, the spin-1/2 AFM trimer chain compounds $A_3Cu_3(PO_4)_4$ (A = Ca,Sr, and Pb) exhibit 1/3 magnetization plateaus [14]. The nature and strengths of the exchange interactions were estimated from the temperature-dependent susceptibility, and the compounds were defined to be good trimer systems with $J_2/J_1 = 0.02$–0.11. The magnetic ordering temperatures for these compounds were found to be low; $T_c = 0.91$ K for Ca, $T_N = 0.91$ K for Sr, and $T_N = 1.26$ K for Pb compounds, respectively. The 1/3 magnetization plateau was also reported for the other spin-1/2 AFM trimer chain compound $Cu_3(P_2O_6OH)_2$ with no magnetic ordering [15,16]. The exchange interactions ($J_2/J_1 \leqslant 0.3$), estimated from bulk susceptibility study, reveal that the compound can be considered as a good trimer system. Among the isostructural compounds from the series $AM_3P_4O_{14}$ (where A = Ca, Sr, Ba, and Pb and M = Ni, Co, and Mn) [17–26], only the $AMn_3P_4O_{14}$ (A = Sr and Ba) compounds with $S = 5/2$ show 1/3 magnetization plateau. However, no magnetization plateau was found for isostructural compounds based on Co- ($S = 3/2$) and Ni- ($S = 1$) having low spin values [17,22], which were predicted to be AFM trimer spin-chain compounds [8]. However, later microscopic investigation of ground-state properties by neutron powder diffraction suggested FM trimers in these compounds [17,22]. For the compounds $ACo_3P_4O_{14}$ and $ANi_3P_4O_{14}$, magnetic long-range ordering temperatures were found to be higher (6.5 and 16 K, respectively [17,22]) in contrast to the $T_N = 2.2$ K for $SrMn_3P_4O_{14}$ [25]. The exchange interactions in $SrMn_3P_4O_{14}$ were estimated by inelastic neutron scattering (INS) study [26], which revealed $SrMn_3P_4O_{14}$ as a good AFM trimer system with negligible intertrimer exchange interaction J_2. The appearance of the 1/3 magnetization plateau was reported due to quantum-mechanical discrete energy levels of the magnetic eigenstates of the spin-5/2 AFM trimer [26]. On the other hand, no such study to estimate the exchange interactions is reported for the Co and Ni-based compounds (where no 1/3 magnetization plateau exists), which could reveal microscopically the reason for the absence of 1/3 magnetization plateau. It is also not known how good or bad $ACo_3P_4O_{14}$ and $ANi_3P_4O_{14}$ compounds are as trimer systems which is defined by the J_2/J_1 ratio. For this purpose, inelastic neutron scattering is one of the best techniques to investigate the nature and strength of the exchange interactions; which can experimentally verify the theoretically predicted criteria for magnetization plateaus, as well as can define the degree of trimerization (how good or bad trimer system) from the J_2/J_1 ratio. The INS measures low-lying magnetic excitations and allows one to determine directly the sign and strength of the possible exchange interactions from the energy/dispersion of the excitations.

Here, we report the results of INS study on the spin-1 trimer chain compound $CaNi_3P_4O_{14}$. The compound $CaNi_3P_4O_{14}$, belonging to the general formula $AM_3P_4O_{14}$ (where A = Ca, Sr, Ba, and Pb and M = Co, Mn, and Ni) [17–26], was initially predicted to show a unique long-range ferrimagnetic ordering due to the periodicity of the exchange interactions [11,26]. The trimer spin chains in $CaNi_3P_4O_{14}$ were estimated, from the bulk magnetization data and Monte Carlo simulations, to be constructed of AFM J_1 and FM J_2 [8]. However, our recent neutron diffraction study [22] evaluated the nature of magnetic ground state as an uncompensated antiferromagnet where spins within trimer unit as well as within the chains have parallel arrangement, suggesting the ferromagnetic type J_1 and J_2 in agreement with the results of recent first-principles calculation [23]. Our neutron diffraction results also reveal a 1D-type magnetic behavior above the T_C. Below the $T_C = 16$ K, in spite of the $S = 1$ trimer chain system, the compound $CaNi_3P_4O_{14}$ is found to be a good realization of a three-dimensional magnet with full ordered moment values of $\sim 2\mu_B/Ni^{2+}$ at 1.5 K. Nuclear magnetic resonance (NMR) study and first-principles calculations on $CaNi_3P_4O_{14}$ suggest an appearance of energy gap in the magnon excitation spectrum in the magnetically ordered state along with a finite orbital degree of freedom associated with the magnetic ordering [23]. NMR data also reveal the presence of anisotropy in the ordered state [23]. In the present work, we have employed inelastic neutron scattering to investigate the magnetic excitations and subsequently the spin Hamiltonian of $CaNi_3P_4O_{14}$. The present work aims to understand the reason for the absence of 1/3 magnetization plateau. The experimental results are corroborated by spin-wave simulations, based on linear spin-wave theory, which reveal the dominance of both the ferromagnetic intratrimer and intertrimer interactions within the given chains. The present study also reveals an antiferromagnetic coupling of the spin chains and presence of a uniaxial single-ion-anisotropy. Our study brings out the role of interchain interactions and magnetocrystalline anisotropy on stabilization of the observed 3D long-range magnetic ordering in the trimer spin-chain compound $CaNi_3P_4O_{14}$. The present study provides an experimental verification of the theoretical predictions for the conditions to observe 1/3 magnetization plateau in spin-trimer chains. The present study also discusses the significance of

the gapless magnetic excitations from the strongly correlated low-dimensional spin chains above the T_C.

II. EXPERIMENTAL DETAILS

Polycrystalline samples of $CaNi_3P_4O_{14}$ (~20 g) were synthesized using a solid-state reaction method in air. Stoichiometric mixture of NiO (99.99%), $CaCO_3$ (99.99%), and $(NH_4)_2HPO_4$ (99.99%) was heated at 1000 °C for 150 h with several intermediate grindings. The phase purity and quality of the sample were verified by x-ray diffraction using a Cu $K_{\alpha 1}$ radiation. Rietveld refinement of the experimental diffraction pattern, using the FULLPROF program [27], confirmed that the samples were single phase with monoclinic crystal structure [space group: $P2_1/c$; lattice parameters $a = 7.3301(2)$ Å, $b = 7.5798(2)$ Å, $c = 9.3929(11)$ Å, and $\beta = 111.989(1)^\circ$] which is consistent with literature reports [20,22].

A low-temperature diffraction pattern at 6 K was recorded by using the neutron powder diffractometer II ($\lambda = 1.2443$ Å) at the Dhruva reactor, Trombay, India. The INS measurements were performed on the high-flux neutron time-of-flight instrument MERLIN at the ISIS facility of the Rutherford Appleton Laboratory, Didcot, United Kingdom. The MERLIN spectrometer has larger detector coverage in both the horizontal (~180°) and vertical (±30°) scattering planes, allowing measurements over large-Q regions of $S(Q,\omega)$ space. About 20-g powder sample was used for the INS measurements. The powder sample was placed in an envelope of thin aluminum foil (40-mm height and 140-mm length), which was rolled into cylindrical form and inserted inside a thin aluminum cylindrical can (diameter of 40 mm with wall thickness of 0.1 mm). The Al can was then mounted into a closed-cycle refrigerator having He-4 exchange gas for low-temperature measurements. The straight Gd slit package was used in the Fermi chopper, which was phased (at a rotation speed of 350 Hz) to allow the recording of spectra with incident energies of 108, 40, 21, and 13 meV, simultaneously, via the rep-rate multiplication method [28,29]. The data were collected at several temperatures between $T = 4$ and 100 K. A typical measurement time for each spectrum was ~3 h. Additional low-energy spectra were collected with an incident energy of 8 meV (at a rotation speed of 300 Hz) at 4, 12, and 18 K with measuring time ~5 h for each run. The data were reduced using the MANTIDPLOT software package [30]. The raw data were corrected for detector efficiency and time-independent background following standard procedures. The spin-wave simulations were carried out using the SPIN-W program [31].

III. RESULTS AND DISCUSSION

A. Crystal structure

The low-temperature crystal structure of $CaNi_3P_4O_{14}$ has been studied by powder neutron diffraction at 6 K. The derived structural parameters were used for the analysis of the low-temperature magnetic excitation spectra. The Rietveld refined diffraction pattern is shown in Fig. 1(a). The Rietveld analysis confirms that $CaNi_3P_4O_{14}$ crystallizes in the monoclinic symmetry (space group $P2_1/c$) with lattice parameters $a = 7.3006(8)$ Å, $b = 7.5462(9)$ Å, $c = 9.3465(10)$ Å, and $\beta = 111.96(7)^\circ$ at 6 K. The crystal structure is found to be similar to that at room-temperature structure [22]. During the refinement, only nuclear phases of $CaNi_3P_4O_{14}$ and $Ni_3P_2O_8$ (a minor secondary phase; wt% ≈ 5%) have been considered. To avoid the influence of the magnetic signal, we have excluded the low-Q region (<2.1 Å^{-1}) data from the refinement. All the atomic sites are considered to be fully occupied and kept fixed during the refinement. In the present crystal structure, there are two independent crystallographic sites for both Ni and P ions, seven independent crystallographic sites for oxygen ions, and a single crystallographic site for Ca ions.

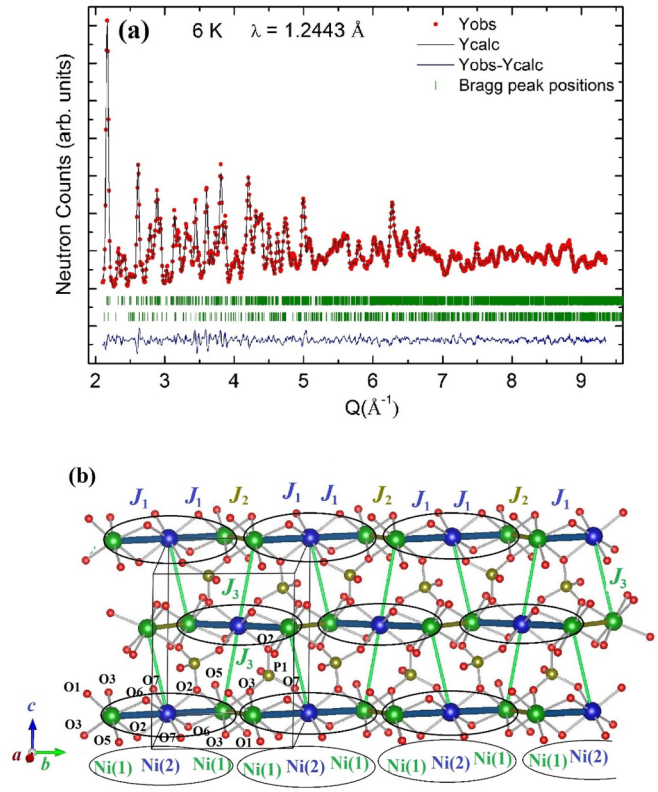

FIG. 1. (a) Experimentally observed (circles) and calculated (line through the data points) neutron diffraction patterns for $CaNi_3P_4O_{14}$ at 6 K over $Q = 2.1$–9.4 Å^{-1}. The difference between observed and calculated patterns is shown by the solid blue line at the bottom. The vertical bars indicate the positions of allowed nuclear Bragg peaks for the main phase $CaNi_3P_4O_{14}$ (top row) and the minor secondary phase $Ni_3P_2O_8$ (bottom row), respectively. (b) A schematic view of the exchange interactions in $CaNi_3P_4O_{14}$. The Ni(1), Ni(2), P, and O ions are shown by green, blue, yellow, and red spheres, respectively. Ca ions are omitted for clarity. The intrachain exchange interactions between Ni(1) and Ni(2) ions are denoted by J_1, whereas between Ni(1) and Ni(1) ions are denoted by J_2. The interchain interaction between two Ni ions having shortest distance ($d_{Ni(1)-Ni(2)} = 4.663$ Å) is shown by J_3. The individual trimer units are marked by ellipsoid.

The spin chains in $CaNi_3P_4O_{14}$ are formed by edge-shared NiO_6 (Ni^{2+}; $3d^8, S = 1$) octahedra along the crystallographic b axis [Fig. 1(b)]. Within a given chain, the special periodicity of the magnetic Ni^{2+} ions Ni(1)-Ni(2)-Ni(1) at two crystallographic independent sites 4e [Ni(1)] and 2a [Ni(2)] results in a spin-trimer structure (J_1-J_1-J_2)

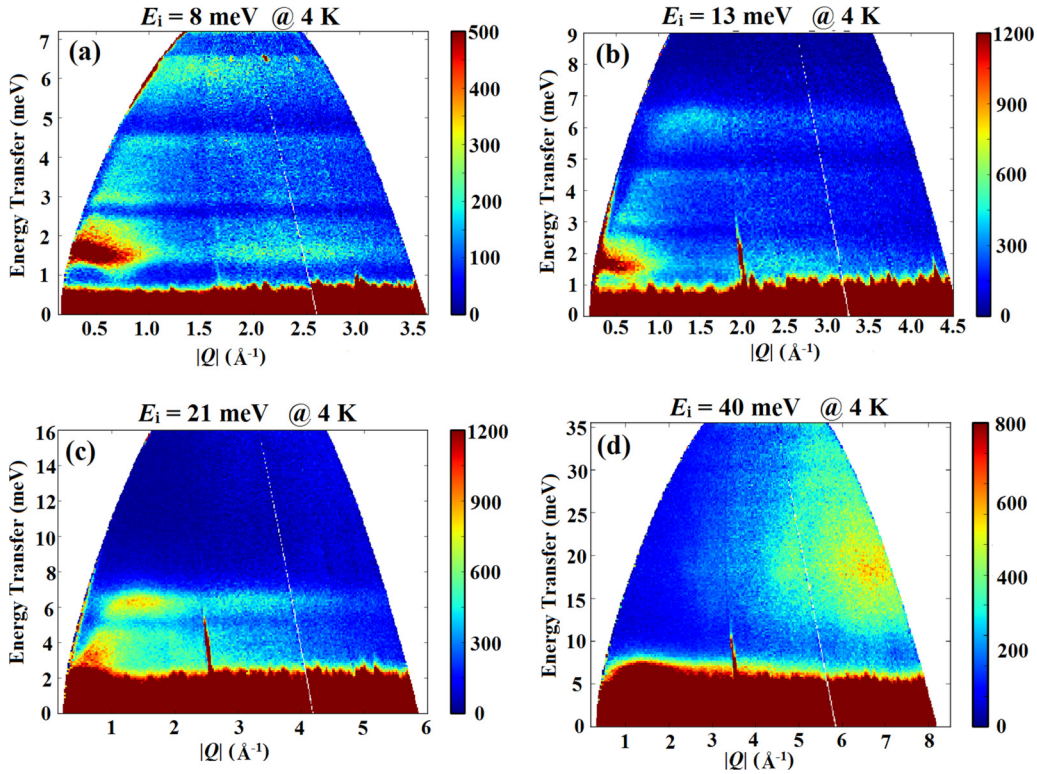

FIG. 2. 2D color map of the INS intensity of $CaNi_3P_4O_{14}$ as a function of energy transfer ($\hbar\omega$) and momentum transfer ($|Q|$), measured at 4 K on the MERLIN spectrometer, with incident neutron energy of $E_i = 8$, 13, 21, and 40 meV. The color scales show the scattering intensity $S(|Q|,\omega)$ in an arbitrary unit. The sharp features with strong intensities (on the lower edge of the spectra, over 5–7 meV for $E_i = 8$ meV, over 1–4 meV for $E_i = 13$ meV, and over 2–8 meV for $E_i = 21$ meV) are experimental artifacts caused by defective detector elements. The sharp feature that is observable at the lower energies around $|Q| \sim 2$ Å^{-1} for $E_i = 13$ meV, $|Q| \sim 2.5$ Å^{-1} for $E_i = 21$ meV, and $|Q| \sim 3.5$ Å^{-1} for $E_i = 40$ meV could be due to some electronic instability in data accusation units in time channels which automatically becomes stable with time [high-temperature patterns above 25 K (Fig. 3)].

having intrachain exchange interactions J_1 [(between Ni(1) and Ni(2); $d_{Ni(1)-Ni(2)} = 3.096(6)$ Å] and J_2 [between Ni(1) and Ni(1); $d_{Ni(1)-Ni(1)} = 3.165(8)$ Å)] with different strengths. The superexchange pathways are Ni(1)-O2-Ni(2) and Ni(1)-O3-Ni(1), respectively. Such spin chains are separated by PO_4 tetrahedra, suggesting weaker interchain exchange interactions. The possible interchain interaction, between two Ni ions from two adjacent chains having shortest distance $d_{Ni(1)-Ni(2)} = 4.663(5)$ Å, is through the superexchange pathway Ni(1)-O3-P1-O2-Ni(2)/Ni(1)-O5-P2-O6-Ni(2) in the bc plane. Moreover, other interchain interactions may also be present between the Ni ions, via PO_4 tetrahedra, having slightly longer distances $d_{Ni(1)-Ni(1)} = 5.036(6)$ Å, $d_{Ni(1)-Ni(2)} = 5.191(4)$ Å and $d_{Ni(2)-Ni(2)} = 6.0063(5)$ Å within the bc plane and $d_{Ni(1)-Ni(1)} = 5.176(8)$ Å in the ab plane, respectively.

B. Spin-wave excitations

The color-coded inelastic neutron scattering intensity maps of $CaNi_3P_4O_{14}$, measured on MERLIN at $T = 4$ K with various incident neutron energies $E_i = 8$, 13, 21, and 40 meV, are shown in Figs. 2(a)–2(d), respectively. All the observable magnetic scatterings are situated below ~6.5 meV. There are three bands of magnetic scatterings over ~1–2.5, ~2.8–4.6, and ~5.3–6.5 meV, respectively. The magnetic character of the scattering is evident from the decreasing intensity with increasing $|Q|$. The magnetic scatterings are found to be extended up to $|Q| \sim 5$Å^{-1}. For the $E_i = 40$-meV spectrum, high-energy scatterings (centered around 20 meV) that appear at high momentum transfer region ($|Q| > 5$ Å^{-1}) are due to the scattering from phonon excitations. Due to the polycrystalline nature of the samples, the scattering cross section $S(|Q|,\omega)$ is powder average of the spin-spin correlation function $S(Q,\omega)$, and it does not carry the information regarding the direction of Q; however, it preserves singularities arising in the density of states as a function of $E = \hbar\omega$. It is found that the powder neutron spectrum contains distinctive fingerprints of the Hamiltonian which can be readily compared to theoretical calculations to obtain approximate parameters.

We have also investigated the temperature variation of the magnetic excitation spectra over a wide temperature range between 4 and 100 K (Figs. 3 and 4). Looking at the temperature evolution of the spectra, the flat magnetic scattering bands appear to be strongly affected by increasing temperature. The intensity of the low-energy bands weakens quickly with increasing temperature. At the same time, the modes soften, and excitation spectra become gapless above the T_C. This implies that the low-$|Q|$ scatterings are related to the spin-wave excitations in the magnetic ordered state (long range) of the material. Weak gapless magnetic excitations persist

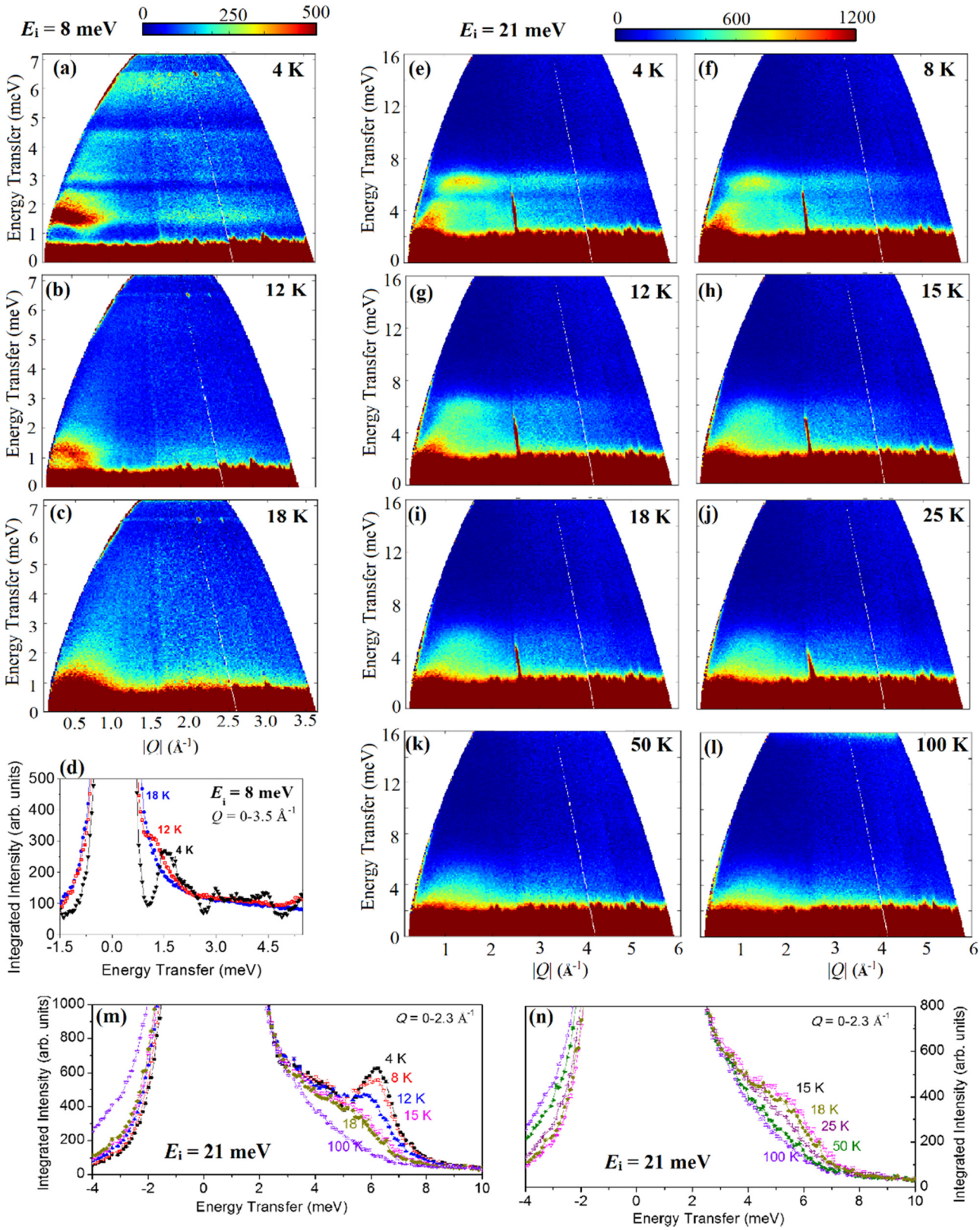

FIG. 3. 2D Color map of the INS intensity of $CaNi_3P_4O_{14}$ as a function of energy transfer ($\hbar\omega$) vs momentum transfer ($|Q|$) measured on the MERLIN spectrometer. (a)–(c) The inelastic spectra measured with incident neutron energy of $E_i = 8$ meV at 4, 12, and 18 K, respectively. (e)–(l) The INS spectra measured with incident neutron energy of $E_i = 21$ meV at 4, 8, 12, 15, 18, 25, 50, and 100 K, respectively. The color scales show the scattering intensity $S(|Q|,\omega)$ in arbitrary units. (d), (m), and (n) The intensity vs energy transfer curves for $E_i = 8$ and 21 meV, respectively. For $E_i = 8$ meV, the intensities were obtained by integrations over $|Q| = 0$–3.5 Å^{-1} and for $E_i = 21$ meV, the integrations were performed over $|Q| = 0$–2.3 Å^{-1}).

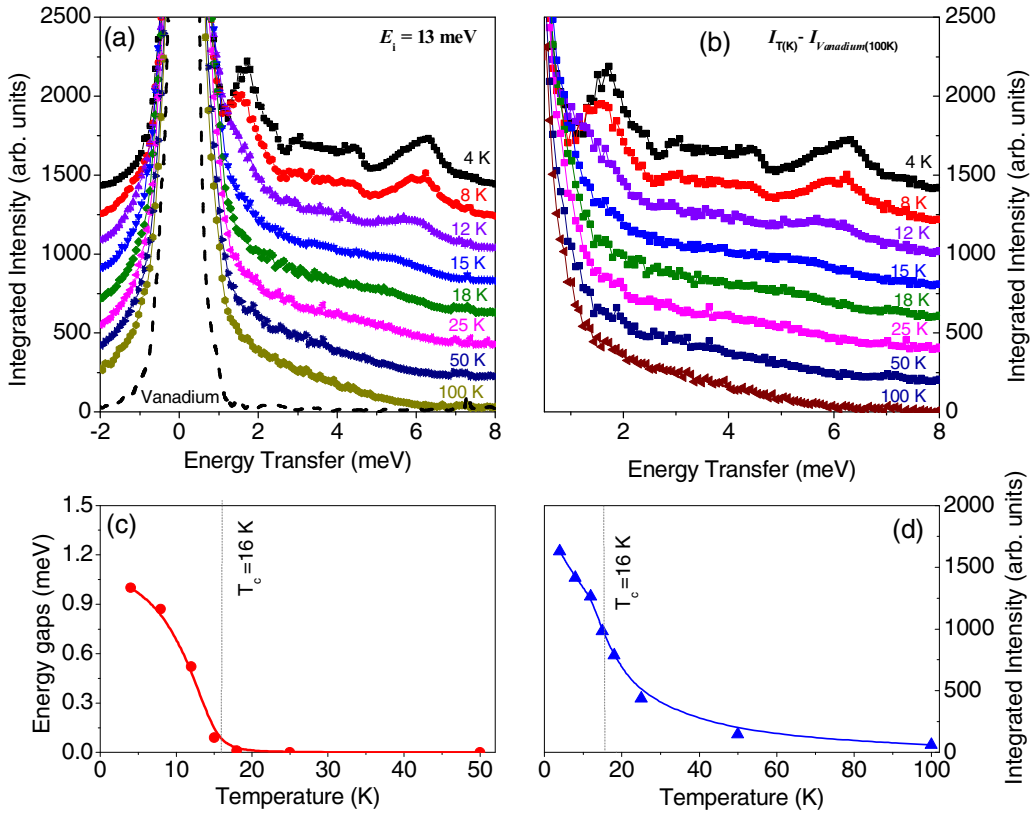

FIG. 4. (a) The measured intensity vs energy transfer curves for $E_i = 13$ meV at different temperatures. The instrumental profile is shown by the dashed line (vanadium curve). The intensities were obtained by integrations over $|Q| = 0$–$1.8\,\text{Å}^{-1}$. The curves are shifted vertically for clarity. (b) The measured curves after subtraction of V curve at 4, 8, 12, 15, 18, 25, and 50 K. (c), (d) The temperature variation of the energy gaps and the integrated intensity, respectively.

above the T_C up to ~100 K (Figs. 3 and 4), which indicates the presence of short-range spin-spin correlations within the chains. Short-range spin-spin correlations were indeed found in neutron diffraction study as reported by us [22]. It may be noted that there are no phonon modes whose intensity increases with increasing temperature around the spin-wave spectra. This makes our data clean and easy to analyze/explain without subtracting the phonon background.

In order to model the experimentally observed magnetic spectrum, we have calculated the spin-wave dispersions, the spin-spin correlation function, and the neutron scattering cross section using the SPINW program [31]. The studied compound $CaNi_3P_4O_{14}$ contains only the magnetic ions Ni^{2+} ($3d^8, S = 1$), and therefore, only interactions between the Ni^{2+} ions need to be considered. Considering the trimer spin-chain crystal structure, we have constructed the magnetic Hamiltonian with three different exchange couplings [shown in Fig. 1(b)] as

$$H = \sum_i \{J_1(\vec{S}_{3i-2}.\vec{S}_{3i-1}) + J_1(\vec{S}_{3i-1}.\vec{S}_{3i}) + J_2(\vec{S}_{3i}.\vec{S}_{3i+1})\} + J_3 \sum_{ij}(\vec{S}_i.\vec{S}_j) + \sum_i D\left(S_i^z\right)^2, \quad (1)$$

where J_1 and J_2 are the nearest-neighbor intrachain exchange interaction between Ni(1) and Ni(2) ions and between Ni(1) and Ni(1) ions, respectively, within a chain. The J_3 is the interchain interactions between two Ni ions from two adjacent chains. Out of many possible interchain interactions having direct distances between 4.663 and 6.0063 (having similar superexchange pathways via Ni-O-P-O-Ni, as discussed in the crystal structure section), we have considered the one having the shortest direct distance $d_{Ni(1)-Ni(2)} = 4.663(5)$ Å [through the superexchange pathways Ni(1)-O3-P1-O2-Ni(2)/Ni(1)-O5-P2-O6-Ni(2) in the bc plane] [Fig. 1(b)]. The last term in Eq. (1) is due to single-ion anisotropy parameter D, which originates from the crystal field of the surrounding oxygen ions in a NiO_6 octahedral environment. The anisotropy parameter D induces a small gap between ground state and excited states, as found in the experimentally measured spectrum [Fig. 5(c)]. For simplicity, we have considered the same D value for both Ni(1) and Ni(2) sites. As the Ni-3d wave functions are very localized, long-range Ni-Ni interactions are neglected. For the simulation of the spin-wave spectra we used the canted magnetic structure as reported earlier by us [22], having a dominated spin component along the c axis and a weak spin component along the b axis. By adjusting the values of the exchange interactions (J_1, J_2, and J_3) and the anisotropy parameter D, a good solution could be found (Table I), and the corresponding simulated excitation pattern is depicted in Fig. 5(b). The simulated energy and momentum cuts are shown in Figs. 5(f) and 5(g) along with that obtained from the measured pattern. An excellent agreement is obtained between the experimentally measured and the model calculated patterns. The major features of the excitation spectra are as

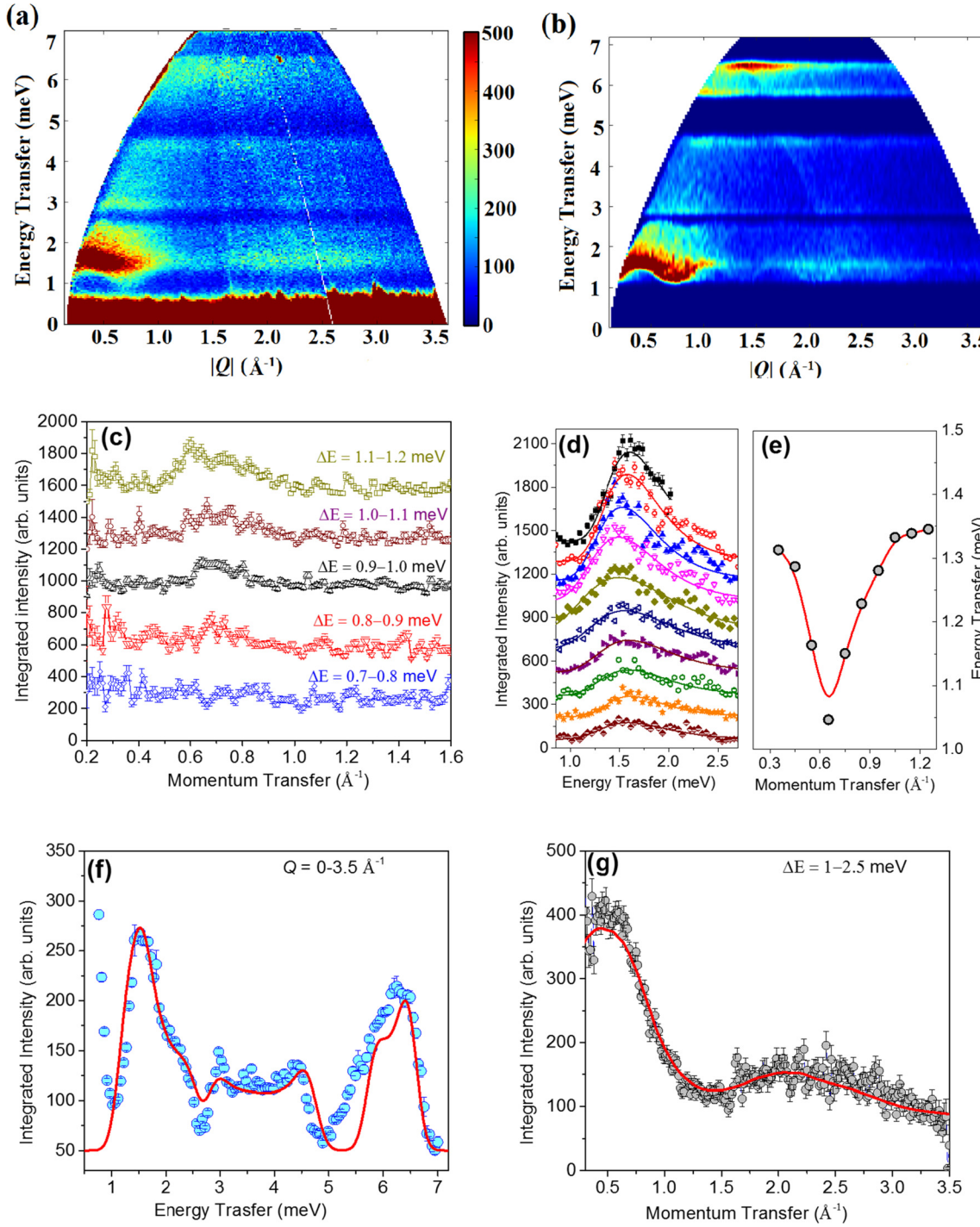

FIG. 5. (a) Experimentally measured (at 4 K) and (b) simulated (by the SPINW program) spin-wave excitation spectra. The strong intensity over 5–7 meV on the lower edge of the experimental spectrum is an artifact caused by defective detector elements. (c) The constant energy cuts as a function of momentum transfer; summed over 0.7–0.8, 0.8–0.9, 0.9–1.0, 1.0–1.1, and 1.1–1.2 meV, respectively. (d) The constant momentum transfer $|Q|$ cuts over the lower edge of the lowest-energy excitation band illustrating the dispersion of the excitation mode. The solid lines are the guide to the eyes. Cuts are taken for $|Q| = 0.35, 0.45, 0.55, 0.65, 0.75, 0.85, 0.95, 1.05, 1.15$, and $1.25\,\text{Å}^{-1}$ with a width of $0.1\,\text{Å}^{-1}$ ($|Q| \pm 0.05\,\text{Å}^{-1}$). (e) The momentum dependence of the lower edge of the lowest-energy band. The experimental scattering intensity as a function of (f) energy transfer (integrated over $|Q|$ range 0–$3.5\,\text{Å}^{-1}$) and (g) momentum transfer (integrated over $\Delta E = 1$–2.5 meV), respectively. The spin-wave calculated intensities (red solid lines) are also plotted for comparison. To match with the experimental intensity, a constant scale factor to the calculated intensity has been applied in addition to a constant background. The addition intensity for the experimental spectra over 5–7 meV in (f) appears from the defective detector elements (for details see caption of Fig. 2).

TABLE I. Possible pathways for intratrimer, intertrimer, and interchain exchange interactions J_1, J_2, and J_3. The Ni-Ni direct distances, bond lengths, and bond angles for the exchange interactions in $CaNi_3P_4O_{14}$ at 6 K. The fitted values of the exchange interactions J's and anisotropy parameter (D) from inelastic neutron scattering spectra at 4 K. All the values of exchange interactions are in meV.

Exchange interaction	Ni…Ni direct distance (Å) and exchange pathways	Bong lengths (Å)	Bond angles (°)	Values (INS) (meV)	Values GGA (meV) [23]	Values GGA+U_{eff} (meV) [23]
J_1	Ni(1)…Ni(2) = 3.096(6) Ni(1)-O2-Ni(2)/ Ni(1)-O6-Ni(2)	Ni(1)-O2 = 2.051(8) Ni(2)-O2 = 2.018(8) Ni(1)-O6 = 2.137(11) Ni(2)-O6 = 2.097(7)	Ni(1)-O2-Ni(2) = 99.1(3) Ni(1)-O6-Ni(2) = 94.0(3)	-1.30 ± 0.05 [FM]	−2.85	−1.54
J_2	Ni(1)…Ni(1) = 3.165(8) Ni(1)-O3-Ni(1)	Ni(1)-O3 = 2.051(9), 2.088(10)	Ni(1)-O3-Ni(1) = 99.8(3)	-1.05 ± 0.05 [FM]	−1.49	−0.578
J_3	Ni(1)…Ni(2)= 4.663(5) Ni(1)-O3-P1-O2-Ni(2)/ Ni(1)-O2-P1-O7-Ni(2)	Ni(1)-O3= 2.088(10) P1-O3 =1.452(12) P1-O2 = 1.515(13) Ni(2)-O2 = 2.018(8) Ni(1)-O2 = 2.051(8) P1-O2 = 1.515(13) P2- O7 = 1.552(14) Ni(2)-O7 = 2.047(8)		0.9 ± 0.1 [AFM]	5.63	2.66
D				-0.25 ± 0.02		

follows: (i) significant bandwidth of the three excitation bands with intermediate gaps [Fig. 5(f)], (ii) a dispersive nature of the bottom edge of the lowest energy band [Figs. 5(d) and 5(e)], (iii) a modulation of the intensity of the lower energy band as a function of momentum transfer $|Q|$ [Fig. 5(g)], and (iv) the presence of an energy gap of about 1 meV between the ground state and the lowest edge of the excitation spectrum as confirmed by the constant energy cuts [Fig. 5(c)].

Our spin-wave simulations reveal that the observed three energy bands correspond to the three spin-wave dispersion modes with distinguished energy ranges. The widths of the energy bands signify the relative strengths of the intrachain interactions (J_1 and J_2). For a model with equal intrachain exchange interactions, i.e., $J_1 = J_2$, the excitation spectra are continuous in energy, i.e., a single band formation from the lowest energy to highest energy (over 1–6.5 meV). In this case, there is no gap present between the three dispersion modes. Any difference in the strength of J_1 and J_2 creates energy gaps between the dispersion modes, resulting in observed three discrete energy bands. The widths of the energy bands and the value of the gaps are proportional to the ratio between the J_1 and J_2. The spin-wave simulations also reveal that the antiferromagnetic interchain interaction J_3 which lies in the bc plane weakly modifies the gaps between the bands. The J_3 also results in a dispersion along the c axis. The main contribution from the J_3 appears at the bottom of the lowest energy band where a clear dispersion is visible in the experimentally measured spectrum at the low-Q region. The fitting suggests that both intratrimer (J_1) and intertrimer (J_2) interactions are ferromagnetic and have almost similar strength; $J_1 = -1.3 \pm 0.05$ meV and $J_2 = -1.05 \pm 0.05$ meV, respectively. The strength of the interchain interaction $J_3 = 0.9 \pm 0.1$ meV is found to be weaker and an antiferromagnetic type. The spin gap of ∼1 meV confirms the presence of a single-ion anisotropy. The anisotropy is found to be along the c axis, i.e., along the moment direction (the easy axis). The fitted value of the single-ion anisotropy parameter D is found to be −0.25 meV. In summary, the fitting of the coupled trimer spin-chain model parameters to the experimental data reveals essential information regarding the magnetism of $CaNi_3P_4O_{14}$. The derived values of the exchange constants show that $CaNi_3P_4O_{14}$ is composed of ferromagnetic trimers that are coupled ferromagnetically along the chain direction (b axis), while such chains are coupled antiferromagnetically.

A comparison between the derived values of exchange coupling parameters from our INS data with the values reported from the density-functional theory (DFT) calculations is given in Table I. The signs of all three exchange interactions obtained from the experiment and DFT calculations are found to be consistent. The dominating interactions are found to be ferromagnetic within the chains through the superexchange pathways Ni(1)-O2-Ni(2)/Ni(1)-O6-Ni(2) and Ni(1)-O3-Ni(2). The ferromagnetic intratrimer and intertrimer interactions in $CaNi_3P_4O_{14}$ could be understood by the Goodenough-Kanamori rule [32,33]. For both the cases, superexchange interactions are between two half-filled Ni-e_g orbitals via superexchange pathways Ni-O-Ni having bond angles (∠Ni-O-Ni∼99°/94° for J_1 and ∠Ni-O-Ni∼100° for J_2) close to 90°. According to the Goodenough-Kanamori rule, the superexchange interactions between two half-filled orbitals connected by a superexchange angle close to 90° always favor a weak ferromagnetic interaction due to the possibility of a direct overlap between two half-filled orbitals (here, Ni-e_g orbitals). Although the signs of the exchange interactions, obtained from both experimental measurements and the DFT calculations, are consistent, their values are found to be significantly different. Experimental data reveal the ratio $J_2/J_1 \sim 0.81$ as compared to ∼0.38–0.52 obtained from the

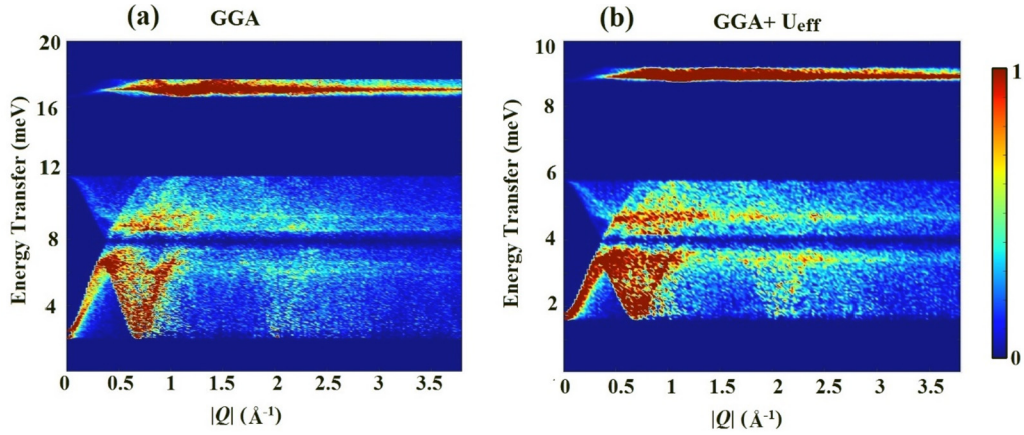

FIG. 6. The powder averaged spin-wave excitation spectra for the values, predicted by the DFT calculation for $CaNi_3P_4O_{14}$, (a) GGA model $J_1 = -2.85, J_2 = -1.49, J_3 = 5.63$ and $D = -0.25$ meV, and (b) GGA+U_{eff} model $J_1 = -1.54, J_2 = -0.578, J_3 = 2.66$ and $D = -0.25$ meV. Color bar represents the intensity in the arb. units.

DFT calculations. Moreover, significant discrepancy has been found for the interchain interaction J_3. The J_3 was predicted, by DFT calculations (by both the GGA (generalized gradient approximation) and GGA+U_{eff} (on site electron-electron interaction)), to be the strongest interaction ($|J_3/J_1| \sim 1.8$–1.9) in spite of the longer superexchange pathways via Ni-O-P1-O-Ni. However, experimental data reveal that the long-range J_3 interaction has a weaker strength ($|J_3/J_1| \sim 0.7$). The spin-wave spectra for the values predicted by the DFT calculations (both the GGA and GGA+U_{eff}) are simulated and shown in Fig. 6. Although the simulated powder-averaged spectra reveal three excitation bands, their individual as well as overall energy range, bandwidth, and intensities are significantly different from the experimental spectra for $CaNi_3P_4O_{14}$ (Fig. 2). This demands further careful DFT-based first-principles calculations, especially proper choice of Hubbard on-site Coulomb correlations and the Hunds exchange parameter (J_H), and proper estimation of charge-transfer energies between different orbitals, with a more accurate crystal structure, and higher plane-wave cutoff energy.

The presence of the energy gap ~1 meV in the magnon excitation spectrum below $T_C = 16$ K is consistent with the reported NMR data that showed a thermally activation behavior of the spin-lattice relaxation rate $1/T_1$ for the P sites [23]. Our spin-wave calculations reveal a single-ion anisotropy with the anisotropy parameter $D = -0.25(2)$ meV. The anisotropy axis is found to be along the c axis, which is the easy axis. The GGA+U+SOC (spin-orbit coupling)-based DFT calculations [23] reveal that the magnetocrystalline anisotropy is weak and favors easy-axis single-ion magnetocrystalline anisotropy, which are consistent with our experimental data. The INS data reveal that the energy gap disappears above the T_C [Fig. 4(c)]. A significant broadening of the excitation bands is also evident above the T_C [Fig. 4(b)]. The sharp change in the single-ion anisotropy indicates that the stability of the 3D magnetic ordering in $CaNi_3P_4O_{14}$ is ascribed to the local magnetic anisotropy in addition to the interchain interactions J_3.

The presence of weak gapless magnetic excitations that persist up to ~100 K is consistent with the previous neutron diffraction study [22], which revealed 1D short-range spin-spin correlations at $T > T_C$. The integrated intensity for the highest energy band is shown in Fig 4(d) as a function of temperature. A significant intensity has been found to persist above $T_C = 16$ K, which is attributed to the magnetic excitation from the strongly correlated spin chains. Our linear spin-wave model indeed reveals a strong coupling along the chains with $|J_3/J_1| \sim 0.69$. The main broad diffuse peak in the neutron diffraction patterns appears over $Q = 0.4 - 1.2$ Å^{-1} and centered around $Q = 0.7$ Å^{-1}. In the present INS data, gapless magnetic excitations appear over a similar Q region above the T_C, revealing the origin as the 1D short-range magnetic ordering and spin fluctuations in the 1D magnetic ordering. The integrated intensity of the diffuse magnetic neutron scattering data also shows a maximum in the vicinity of the T_C. The NMR data [23] also revealed a change of the ratio $(1/T_1)/(1/T_2)$ (T_2 = spin-spin relaxation rate) (which actually gives the ratio of dynamical susceptibility $\chi_\perp$ and $\chi_\parallel$) below 50 K. Such one-dimensional spin-spin correlations [34] may lead to exotic physical properties, such as magnetodielectric coupling above 3D ordering temperature as reported for the spin-chain compound $Ca_3Co_2O_6$ [35], and hence opens up opportunities for further studies.

Now we compare the microscopic magnetic model of $CaNi_3P_4O_{14}$ with that of the isostructural compound $SrMn_3P_4O_{14}$ [24–26,36], which shows a 1/3 magnetization plateau. For $SrMn_3P_4O_{14}$, the intratrimer exchange interaction J_1 was estimated to be antiferromagnetic ($J_1 = 0.29$ meV) and the intertrimer exchange interaction J_2 was also concluded to be antiferromagnetic, however very weak. Therefore, $SrMn_3P_4O_{14}$ could be considered as a good spin-trimer compound where trimers are nearly isolated. The excitations of $SrMn_3P_4O_{14}$ are composed of discrete energy levels of the magnetic eigenstates (with S^{tot} extending up to 15/2) of the spin-5/2 AFM trimer [24–26]. The ground states of such $S = 5/2$ trimer system are sixfold degenerated and can have a finite magnetic moment. The origin of the 1/3 magnetization plateau in $SrMn_3P_4O_{14}$ was reported to be arising from the quantum-mechanical discrete energy levels of the spin trimer. In weak magnetic fields, the degeneracy is removed and $S^z = +5/2$ becomes the ground state which saturates under an external magnetic field of around 2 T showing the 1/3 magnetization plateau for field values up to 10.6 T. This 1/3

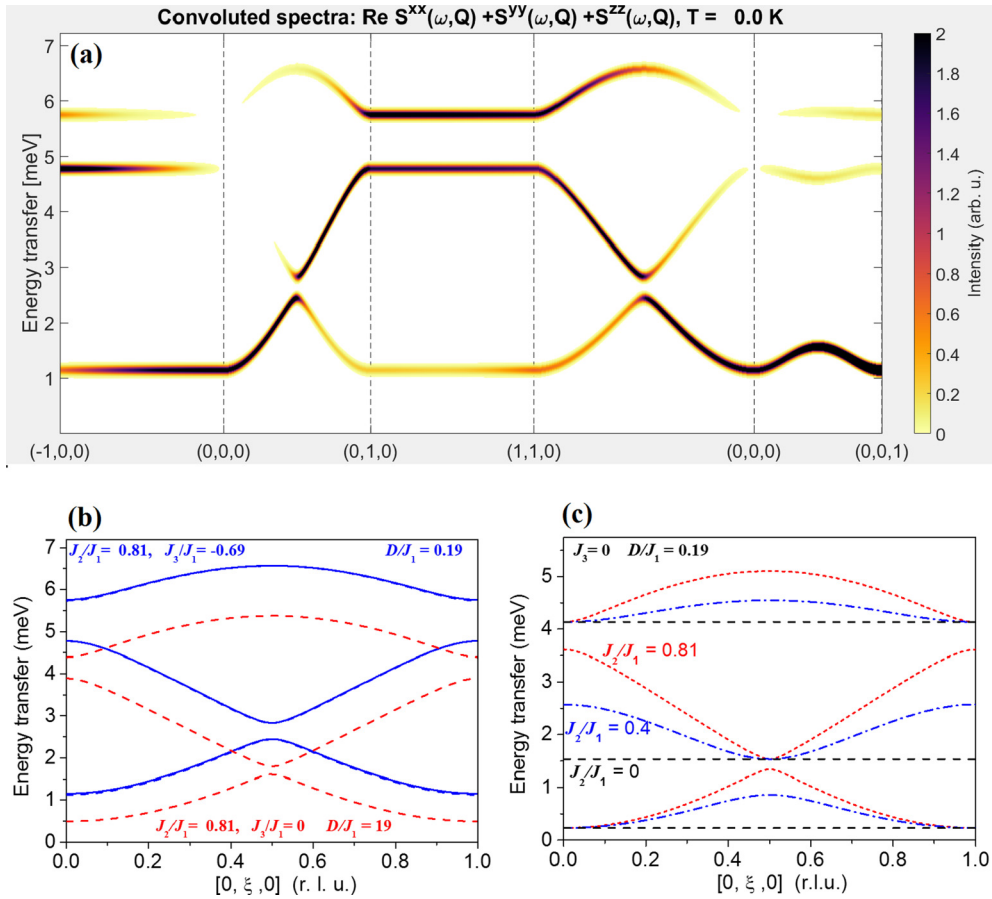

FIG. 7. (a) The simulated dispersion curves along the different crystallographic directions with the derived parameters $J_1 = -1.3$, $J_2 = -1.05$, $J_3 = 0.9$, and $D = -0.25$ meV. The intensity variation of the dispersion patterns shown by the color map. (b) The dispersion curves (solid blue lines) along the chain direction (b axis) with the derived parameters $J_2/J_1 = 0.81$, $J_3/J_1 = -0.69$, and $D/J_1 = 0.19$. The dashed curves represent the nature of the dispersion curves in the absence of the interchain interactions ($J_3 = 0$). (c) The variation of the dispersion curves with J_2/J_1 and $J_3 = 0$. Discrete energy levels are evident for $J_2 = 0$.

magnetization plateau occurs due to the energy gap between the plateau state ($S^{\text{tot}} = 5/2$) and the higher energy state ($S^{\text{tot}} = 7/2$) that prevents the magnetization from increasing with magnetic field [24–26]. On the other hand, the spin model of the present isostructural compound $CaNi_3P_4O_{14}$ can be defined as ferromagnetic trimer chains (FM-FM-FM) ($J_2/J_1 \sim 0.81$) with a strong interchain antiferromagnetic coupling. The ferromagnetic spin-chain configuration gives dispersive spin-wave excitation spectra, as evident from our experimental study (Figs. 5 and 7). In this case, no magnetization plateau is expected. A variation of the dispersion curves with the J_2/J_1 is shown in Fig. 7(c), which reveals that with decreasing J_2 value the bandwidths of the dispersion modes decrease and subsequently the gaps between them increase. For $J_2 = 0$, the modes become dispersionless and as a result, the excitations consist of discrete energy states. These discrete energy levels are different from the eigenstates of an isolated spin trimer, such as in $SrMn_3P_4O_{14}$. The exact nature of the energy spectrum of an isolated spin trimer can be obtained only by quantum calculations (using an exact diagonalization method). As outlined in the Introduction, for $S = 1$ FM trimer chains, the 1/3 and 2/3 magnetization plateaus are expected only when the FM trimers (J_1 FM) are coupled antiferromagnetically (J_2 AFM), i.e., spin chain with FM-FM-AFM periodicity, and the ratio $|J_2/J_1|$ is above a critical value (when the AFM coupling becomes more dominant) [11]. The required conditions are not fulfilled by the present $CaNi_3P_4O_{14}$ compound as J_2 is ferromagnetic. However, with a proper crystal modification, the magnetization plateaus state may be possible to introduce in a spin trimer chain compound like $CaNi_3P_4O_{14}$. In the present compound the superexchange interaction J_2 is through the pathway Ni(1)-O3-Ni(1) involving a bond angle Ni(1)-O3-Ni(1) of 99.8(3)°, which is favorable for ferromagnetism as per the Goodenough-Kanamori rule. The sign of J_2 can be modified from ferromagnetic to antiferromagnetic by an increase of the bond angle Ni(1)-O3-Ni(1). For the J_2 superexchange interactions, two neighboring magnetic Ni(1) ions are connected by two O3 ions in two different paths. Each O3 ions is connected to a P(1)O4 tetrahedron as shown in Fig. 8. Thus, a replacement of P1 ion by a larger ion of similar type such as arsenic (As) will increase the As–O3 bond length. This in turn is expected to push the O3 ions from both the sides as shown by arrows in Fig. 8, and subsequently it causes an increase of the bond angle Ni(1)-O3-Ni(1). The present experimental study also reveals a strong interchain exchange interaction ($|J_3/J_1| \sim 0.7$) in $CaNi_3P_4O_{14}$, which leads to the observed higher 3D long-range ordering temperature $T_C =$ 16K as compared to that for the isostructural compounds

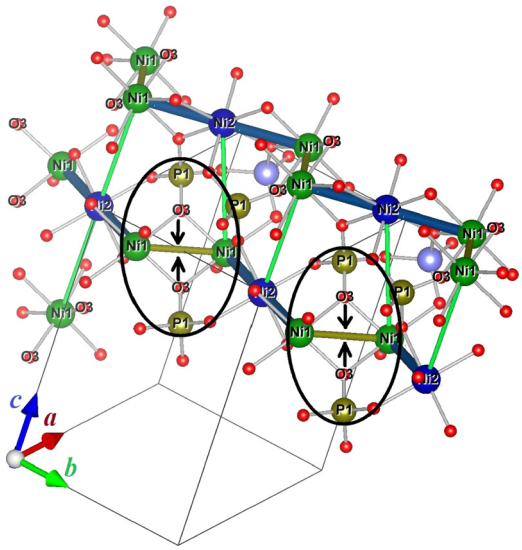

FIG. 8. The local crystal structure of $CaNi_3P_4O_{14}$ highlighting (by solid ovals) the inter trimer superexchange interaction J_2. The arrows indicate the possible movements of the O3 ions upon substitution of a larger ion of similar type such as arsenic (As) at the P1 position.

[$T_N = 6.5$ and 2.2 K for Co and Mn ($J_3/J_1 < 10^{-3}$)-based compounds, respectively]. Figure 7(b) shows the effect of interchain interaction J_3 on the excitation spectra. The strong interchain exchange interaction J_3 also results into the full ordered moment values of 1.98 and 1.96 μ_B/Ni^{2+} at 1.5/K [theoretical value is $2\mu_B/Ni^{2+}(S = 1)$] for the present compound. The spin-1 chain system, $CaNi_3P_4O_{14}$, is therefore found to be a good realization of a 3D magnetic system below $T_C = 16$ K with a negligible effect of quantum fluctuations.

IV. SUMMARY AND CONCLUSION

We have performed inelastic neutron scattering measurements on the spin-1 trimer chain compound $CaNi_3P_4O_{14}$, which reveal gapped dispersive spin-wave excitations at low temperatures ($T < T_C$). The magnetic excitations partially survive at temperatures (up to ~100 K) much above the $T_C = 16$ K (of long-range 3D order), indicating the dominating 1D magnetic interactions. We performed the quantitative analysis of the observed magnetic excitation spectra using the linear spin-wave calculations. The fitting of the coupled trimer spin-chain model parameters to the experimental data reveals essential information regarding the magnetism of $CaNi_3P_4O_{14}$. Our spin-wave analysis indicates that the stronger exchange interactions are within the chain along the b axis. The signs of the exchange interactions are in agreement with the reported DFT calculations. However, disagreements have been found on the strength of the interactions. The strengths of both the ferromagnetic intratrimer (J_1) and intertrimer (J_2) nearest-neighbor exchange interactions are found to be similar ($J_2/J_1 \sim 0.81$), which is in contrast to the predicted values ($J_2/J_1 \sim 0.38$–0.52) by the DFT calculations. Moreover, the DFT study predicted a strongest interchain interaction ($|J_3/J_1| \sim 1.8$–1.9), which is in contrast to our inelastic neutron scattering results that reveal a weaker J_3 ($|J_3/J_1| \sim 0.69$). The derived weaker J_3 is consistent with the spin-chain-type crystal structure. Nevertheless, the relatively strong value of the J_3 leads to the conventional 3D-type magnetic ordering behavior below the T_C with full ordered moment for Ni^{2+} ions at 1.5 K in the present spin-1 trimer chain compound $CaNi_3P_4O_{14}$. Furthermore, the observation of a spin gap below the T_C is due to a weak single-ion anisotropy ($D = -0.25$ meV). The sharp change of single-ion anisotropy across the T_C reveals that the stability of the 3D magnetic ordering in $CaNi_3P_4O_{14}$ is ascribed to the local magnetic anisotropy in addition to the interchain interactions. The present study determines the spin Hamiltonian for the trimer spin-chain compound $CaNi_3P_4O_{14}$, which not only explains the observed physical properties in $CaNi_3P_4O_{14}$ but also explains why the 1/3 quantum magnetization state is present only for few members across the series of the isostructural compounds. The present study can foster research on the magnetic excitations in this class of spin-chain materials with multiple intrachain interactions and would generate theoretical interest in the development of a more realistic model to understand the complex magnetic behaviors. Besides, the observed gapless magnetic excitations up to a higher temperature of $T/T_C \sim 6$ generates interest to look for unexplored physical properties, such as magnetodielectric and magnetothermal properties.

ACKNOWLEDGMENTS

A.K.B. and S.M.Y. thank K. Ghoshray for scientific discussion on the present compound. A.K.B. also acknowledges the help received from H. C. Walker on the determination of the instrumental resolution of the MERLIN spectrometer.

[1] T. Giamarchi, *Quantum Physics in One Dimension* (Oxford University Press, Oxford, 2003).
[2] F. D. M. Haldane, Continuum dynamics of the 1-D Heisenberg antiferromagnet: Identification with the O(3) nonlinear sigma model, Phys. Lett. A **93**, 464 (1983).
[3] F. D. M. Haldane, Nonlinear Field Theory of Large-Spin Heisenberg Antiferromagnets: Semiclassically Quantized Solitons of the One-Dimensional Easy-Axis Neel State, Phys. Rev. Lett. **50**, 1153 (1983).
[4] T. Sakai and M. Takahashi, Effect of the Haldane gap on quasi-one-dimensional systems, Phys. Rev. B **42**, 4537 (1990).
[5] A. K. Bera, B. Lake, A. T. M. N. Islam, O. Janson, H. Rosner, A. Schneidewind, J. T. Park, E. Wheeler, and S. Zander, Consequences of critical interchain couplings and anisotropy on a Haldane chain, Phys. Rev. B **91**, 144414 (2015).
[6] J. C. Bonner, S. A. Friedberg, H. Kobayashi, D. L. Meier, and H. W. J. Blote, Alternating linear-chain antiferromagnetism in copper nitrate $Cu(NO_3)_2.2.5H_2O$, Phys. Rev. B **27**, 248 (1983).
[7] G. Castilla, S. Chakravarty, and V. J. Emery, Quantum Magnetism of $CuGeO_3$, Phys. Rev. Lett. **75**, 1823 (1995).
[8] M. Hase, H. Kitazawa, N. Tsujii, K. Ozawa, M. Kohno, and G. Kido, Ferrimagnetic long-range order caused by periodicity

of exchange interactions in the spin-1 trimer chain compounds $ANi_3P_4O_{14}$ (A = Ca, Sr, Pb, Ba), Phys. Rev. B **74**, 024430 (2006).

[9] M. Hagiwara, Y. Narumi, K. Minami, K. Kindo, H. Kitazawa, H. Suzuki, N. Tsujii, and H. Abe, Magnetization process of an $S = 1/2$ tetramer chain with ferromagnetic-ferromagnetic-antiferromagnetic-antiferromagnetic bond alternating interactions, J. Phys. Soc. Jpn. **72**, 943 (2003).

[10] Y.-T. Oh, H. Katsura, H.-Y. Lee, and J. H. Han, Proposal of a spin-one chain model with competing dimer and trimer interactions, Phys. Rev. B **96**, 165126 (2017).

[11] B. Gu, G. Su, and G. Song, Magnetic properties of J-J-J' quantum Heisenberg chains with spin $S = 1/2$, 1, 3/2 and 2 in a magnetic field, J. Phys.: Condens. Matter **17**, 6081 (2005).

[12] H. J. Schmidt and J. Richter, Exact ground states for coupled spin trimers, J. Phys. A: Math. Theor. **43**, 405205 (2010).

[13] W. J. Caspers and G. I. Tielen, Rotational ordering and symmetry breaking in the triangular antiferromagnetic Heisenberg lattice, Phys. A (Amsterdam, Neth.) **135**, 519 (1986).

[14] A. A. Belik, A. Matsuo, M. Azuma, K. Kindo, and M. Takano, Long-range magnetic ordering of S = 1/2 linear trimers in $A_3Cu_3(PO_4)_4$ (A = Ca, Sr, and Pb), J. Solid State Chem. **178**, 709 (2005).

[15] M. Hase, M. Kohno, H. Kitazawa, N. Tsujii, O. Suzuki, K. Ozawa, G. Kido, M. Imai, and X. Hu, 1/3 magnetization plateau observed in the spin-1/2 trimer chain compound $Cu_3(P_2O_6OH)$, Phys. Rev. B **73**, 104419 (2006).

[16] M. Hase, M. Matsuda, K. Kakurai, K. Ozawa, H. Kitazawa, N. Tsujii, A. Danni, M. Kohno, and X. Hu, Direct observation of the energy gap generating the1/3 magnetization plateau in the spin-1/2 trimer chain compound $Cu_3(P_2O_6OD)_2$ by inelastic neutron scattering measurements, Phys. Rev. B **76**, 064431 (2007).

[17] M. Hase, V. Yu. Pomjakushin, A. Danni, and H. Kitazawa, Magnetic structure of $SrCo_3P_4O_{14}$ determined from neutron powder diffraction results, J. Phys. Soc. Jpn. **81**, 064702 (2012).

[18] B. El-Bali, A. Boukhari, J. Aride, K. Maass, D. Wald, R. Glaum, and F. Abraham, Crystal structure and colour of $SrNiP_2O_7$ and $SrNi_3(P_2O_7)_2$, Solid State Sci. **3**, 669 (2001).

[19] T. Yang, Y. Zhang, S. Yang, G. Li, M. Xiong, F. Liao, and J. Lin, Four isomorphous phosphates $AM_3P_4O_{14}$(A = Sr,Ba; M = Co,Mn) with antiferromagnetic-antiferromagnetic-ferromagnetic trimerized chains, showing 1/3 quantum magnetization plateaus only in the manganese(II) system, Inorg. Chem. **47**, 2562 (2008).

[20] K. H. Lii, P. F. Shih, and T. M. Chen, $AM_3(P_2O_7)_2$(A = alkaline-earth metals; M - iron, cobalt, nickel): Diphosphates containing infinite chains of edge-sharing MO_6 octahedra, Inorg. Chem. **32**, 4373 (1993).

[21] A. Elmarzouki, A. Boukhari, A. Berrada, and E. M. Holt, Crystal structures of isotypical diphosphates $PbCo_3(P_2O_7)_2$ and $PbFe_3(P_2O_7)_2$, J. Solid State Chem. **118**, 202 (1995).

[22] A. K. Bera, S. M. Yusuf, A. Kumar, M. Majumder, K. Ghoshray, and L. Keller, Long-range and short-range magnetic correlations, and microscopic origin of net magnetization in the spin-1 trimer chain compound $CaNi_3P_4O_{14}$, Phys. Rev. B **93**, 184409 (2016).

[23] M. Majumder, S. Kanungo, A. Ghoshray, M. Ghosh, and K. Ghoshray, Magnetism of the spin-trimer compound $CaNi_3(P_2O_7)_2$: Microscopic insight from combined P-NMR and first-principles studies, Phys. Rev. B **91**, 104422 (2015).

[24] M. Hase, T. Yang, R. Cong, J. Lin, A. Matsuo, K. Kindo, K. Ozawa, and H. Kitazawa, High-field magnetization of $SrMn_3P_4O_{14}$ exhibiting a quantum-mechanical magnetization plateau and classical magnetic long-range order, Phys. Rev. B **80**, 054402 (2009).

[25] M. Hase, V. Y. Pomjakushin, L. Keller, A. Daenni, O. Sakai, T. Yang, R. Cong, J. Lin, K. Ozawa, and H. Kitazawa, Spiral magnetic structure in spin-5/2 frustrated trimerized chains in $SrMn_3P_4O_{14}$, Phys. Rev. B **84**, 184435 (2011).

[26] M. Hase, M. Matsuda, K. Kaneko, N. Metoki, K. Kakurai, T. Yang, R. Cong, J. Lin, K. Ozawa, and H. Kitazawa, Magnetic excitations in the spin-5/2 antiferromagnetic trimer substance $SrMn_3P_4O_{14}$, Phys. Rev. B **84**, 214402 (2011).

[27] J. Rodriguez-Carvajal, Recent advances in magnetic structure determination by neutron powder diffraction, Phys. B: Condens. Matter **192**, 55 (1993).

[28] M. Russina and F. Mezei, First implementation of repetition rate multiplication in neutron spectroscopy, Nucl. Instrum. Methods Phys. Res., Sect. A **604**, 624 (2009).

[29] M. Nakamura, R. Kajimoto, Y. Inamura, F. Mizuno, M. Fujita, T. Yokoo, and M. Arai, First demonstration of novel method for inelastic neutron scattering measurement utilizing multiple incident energies, J. Phys. Soc. Jpn. **78**, 093002 (2009).

[30] O. Arnold, J. C. Bilheux, J. M. Borreguero, A. Buts, S. I. Campbell, L. Chapon, M. Doucet, N. Draper, R. Ferraz Leal, M. A. Gigg, V. E. Lynch, A. Markvardsen, D. J. Mikkelson, R. L. Mikkelson, R. Miller, K. Palmen, P. Parker, G. Passos, T. G. Perring, P. F. Peterson, S. Ren, M. A. Reuter, A. T. Savici, J. W. Taylor, R. J. Taylor, R. Tolchenov, W. Zhou, and J. Zikovsky, Mantid-data analysis and visualization package for neutron scattering and muSR experiments, Nucl. Instrum. Methods Phys. Res., Sect. A **764**, 156.

[31] S. Toth and B. Lake, Linear spin wave theory for single-Q incommensurate magnetic structures, J. Phys.: Condens. Matter **27**, 166002 (2015).

[32] J. B. Goodenough, Theory of the role of covalence in the perovskite-type manganites [La,M(II)]MnO_3, Phys. Rev. **100**, 564 (1955).

[33] J. B. Goodenough, *Magnetism and the Chemical Bond* (Interscience-Wiley, New York, 1963).

[34] A. Jain, P. Y. Portnichenko, H. Jang, G. Jackeli, G. Friemel, A. Ivanov, A. Piovano, S. M. Yusuf, B. Keimer, and D. S. Inosov, One-dimensional dispersive magnon excitation in the frustrated spin-2 chain system $Ca_3Co_2O_6$, Phys. Rev. B **88**, 224403 (2013).

[35] T. Basu, K. K. Iyer, P. L. Paulose, and E. V. Sampathkumaran, Dielectric anomalies and magnetodielectric coupling behavior of single crystalline $Ca_3Co_2O_6$, a geometrically frustrated magnetic spin-chain system, J. Alloys Compd. **675**, 364 (2016).

[36] M. Hase, A. Donni, K. Ozawa, H. Kitazawa, O. Sakai, V. Y. Pomjakushin, L. Keller, K. Kaneko, N. Metoki, K. Kakurai, M. Matsuda, T. Yang, R. Cong, and L. Jianhua, Neutron scattering studies of the spin-5/2 antiferromagnetic linear trimer substance $SrMn_3P_4O_{14}$, J. Phys.: Conf. Ser. **340**, 012066 (2012).